IC/89/23
INTERNAL REPORT
(Limited Distribution)

International Atomic Energy Agency
and
United Nations Educational Scientific and Cultural Organization
INTERNATIONAL CENTRE FOR THEORETICAL PHYSICS

# PHYSICS OF THE TROPOSPHERIC RADIOPROPAGATION*

G.O. Ajayi**
International Centre for Theoretical Physics, Trieste, Italy.

MIRAMARE – TRIESTE
February 1989

* To be published in the Proceedings of the ICTP College on Theoretical and Experimental Radiopropagation Physics, 6–24 February 1989, Trieste, Italy.

** Permanent address: Department of Electronic and Electrical Engineering, Obafemi Awolowo University, Ile-Ife, Nigeria.

## Table of Contents

# 1. INTRODUCTION

The troposphere is the lower part of the Earth's atmosphere extending to an altitude of about 9 km at the earth's poles and 17 km at the equator. The tropopause is the upper boundary of the troposphere, above which the temperature increases slightly with height or remains constant.

The percentage composition of the principal gases does not change with altitude except that of water vapour. The permanent dipole moment of the molecules of water vapour causes it to be a very significant contributor to the variability of the atmospheric refractive index. The proportion by volume of water vapour in the air at the ground level on the average varies from less than 0.001% in the arctic to more than 6% in the tropics [12]. This proportion decreases rapidly with height and is highly dependent on local air temperature. Fig. 1 shows [29] typical variations in Niger, West Africa. Radiation, absorption, condensation, evaporation, advection, convection, turbulent diffusion and a number of complex and interacting meteorological phenomena lead to non-linear and fairly unpredictable processes in the troposphere [34].

The troposphere is transparent to most of the solar energy, hence the source of the heat for the troposphere is the Earth which is heated by the sun. The Earth heats the troposphere through the processes of conduction, convection and radiation. The resulting thermal structure is modified by the water vapour generated from ocean surfaces and large bodies of water. The dry adiabatic lapse rate in the troposphere is 9.8°C per km. Due to the presence of water vapour, the temperature lapse rate is less than 9.8°C per km. The temperature in the troposphere gradually decreases with height at the rate of approximately 6°C per km.

Temperature increases with altitude in an inversion layer and such a layer is highly stable. All vertical motions are strongly inhibited and pollution emitted below the layer tends to be confined below it. Radiation cooling is one of the causes of temperature inversion. Advection can also cause temperature inversion. For example, hot dry air from land may move over cold wet air causing temperature inversion.

## 2. RADIO REFRACTIVE INDEX

The atmospheic radio refractive index, $n$ is very close to unity (typically 1.00035), hence it is more convenient to talk of the refractivity, $N$ given by

$$N = (n-1) \times 10^6 = \frac{77.6}{T}(P + 4810\frac{e}{T}) \quad (1)$$

where

$P =$ atmospheric pressure (mb)

$e =$ water vapour pressure (mb)

$T =$ absolute temperature (K)

The relationship between water vapour density, $\rho(gm/m^3)$, water vapour pressure, $e(mb)$ and the relative humidity, $H(\%)$ is given by Ref. 8.

$$\rho = 216.7\frac{e}{T} \quad (2)$$

$$H = 100 \cdot e/e_s \quad (3)$$

$$e_s = \frac{5854}{T^5} \cdot 10^{(20-2950/T)} \quad (4)$$

where $e_s$ = saturation vapour pressure (mb) at temperature T(K).

The dependence of refractivity on temperature and relative humidity is very important in the tropics. Fig. 2 illustrates [34] these changes in refractivity for varying relative humidity values at different temperatures. For example, at a relative humidity of 60%, when the temperature changes from $-10°C$ to $+10°C$ the variation in refractivity is negligible in contrast to a much larger variation at higher temperatures, say from 20°C to 40°C. This pattern explains how surface refractivity and also the effective earth's radius factor (k) may be subjected to wild variations in a single day in the tropical region.

### 2.1 Refractivity in the Model Atmosphere

Pressure, temperature and water vapour contents all decrease with height above the earth's surface in the troposphere on the average, except in temperature inversion layers where temperature increases with height.

$N$ varies with height as

$$N(h) = N_s \exp(-h/H) \quad (5)$$



where $N(h)$ is refractivity at a height $h$ above which the refractivity is $N_s$, $H$ is scale height.

For the CCIR model atmosphere [6]

$$N(h) = 315\exp(-0.136h) \quad (6)$$

where 315 is the average surface refractivity and the scale height is 7.353 km. $h$ is in km.

### 2.2 Sea Level Refractivity

For prediction of some propagation effects, the surface refractivity is useful. To remove surface height variations (topography of location) surface refractivity can be reduced to sea-level values $N_0$ using

$$N_s = N_0 \exp(-0.136h) \quad (7)$$

The scale height in the locality can be used if available.

The CCIR has produced world map of $N_0$. Figs. 3(a) and (b) [17] show the surface refractivity variation in Africa, with the following main features [28].

(a) In the equatorial climatic belt ($\pm 5°$ latitude) $N_0$ is characterized by high values in the range 370 to 390 $N$ units and is practically independent of season. The annual range of mean $N_0$ is only about $5 - 10N$ units.

(b) In the tropical continental climatic region ($5° - 20°$ latitude), $N_0$ is much higher during the rainy season than during the dry season and there are high annual ranges of about 70–110 N units.

(c) In the hot desert region ($20° - 30°N$ latitude), low values of about 310 are found in the hinterland.

(d) In the warm temperate region, moderate values of $N_0$ (300 – 350) $N$ units are found with a low annual range of about 5N units.

Owolabi and Williams [26] have shown that in Nigeria, $N_s$ decreases from the south to the north and the values 375, 350 and 325 N units were obtained for the southern (latitude $4° - 7°$ N), middle (latitude 10° - 13°N) zones respectively. In Brazil, the values of $N_0$ at Belem (1.5°S, 48.5°W) are about 370 and 360 N units in February and August, respectively, indicating slightly greater refractivity in local summer which coincides with the rainy season [30],[32].

## 2.3 Refractivity Gradient

The curvature of the ray path in the troposphere is determined by the refractivity gradient and not by its absolute value. Making use of the standard (average) gradients of pressure, temperature and water vapour at ground level for temperate latitutes, we have

$$\frac{dN}{dh} = -40N/km \tag{8}$$

In a temperature inversion, when $dT/dh$ is positive, $dN/dh$ becomes negatively large. Since temperature inversion inhibits vertical motion and mixing, a large lapse rate of water vapour is usually produced in such layers. The combination of positive $dT/dh$ and a large negative $de/dh$ results in large negative values of refractivity gradient in an inversion layer.

## 2.4 Atmospheric Refraction

A radio wave encounters variations in atmospheric refractive index along its trajectory that cause the ray path to become curved.

The radius of curvature $R$ of the ray is given by

$$\frac{1}{R} = -\frac{1}{n}\frac{dn}{dh}\cos\theta \tag{9}$$

where $\theta$ = angle of the radio ray with the horizontal.

In the troposphere, $n \approx 1$ and for small values of angle $\theta$, we have

$$\frac{1}{R} = -\frac{dn}{dh} = -\frac{dN}{dh} \times 10^{-6} \tag{10}$$

$R$ is determined by the lapse rate of refractive index with height and not by its absolute value. When $dN/dh$ is negative, $R$ is positive and the propagation path is convex.

**2.4.1 Effective earth radius** A hypothetical effective earth radius that makes the relative curvature of the ray and that of an effective earth to be such that radio rays appear to travel in straight lines rather than curved lines over the true earth. This technique is adequate in a well mixed atmosphere where the refractivity gradient can be assumed to be constant with height.



By equating the relative curvatures, we have

$$a' = ka \tag{11a}$$

where

$$k = \left(1 + a\frac{dN}{dh} \times 10^{-6}\right)^{-1} \tag{11b}$$

where $k$ is the effective earth radius factor. For middle latitudes, average $dN/dh$ for standard atmosphere is $-40N$ units/km and $k$ is 4/3. There is a large variation in the median values of $k$ near the equator. In the equatorial regions of India, $k$ varies between 1.3 and 1.8 [28]. In the equatorial regions of Africa, $k$ is 1.5 [17]. $k$ was also found to be 1.43 and 1.22 for the rainy and dry seasons, respectively, and $k$ of 1.20 was obtained for the desert region in Africa.

**2.4.2 M-profile** The $M$-profile technique is useful for a stratified troposphere when the refractivity gradient is no longer constant with height. The term $M$ or "modified" refractive index has been defined in units which relate the curvature of microwave beam to the curvature of the earth

$$M = N + 10^6\frac{h}{a} \tag{12a}$$

or

$$M = N + 157h \tag{12b}$$

Fig. 4 shows typical $M$-profiles [19]

$$\frac{dM}{dh} = \frac{dN}{dh} + 157 \tag{13}$$

i.e. $\frac{dM}{dh}$ is positive for $\frac{dN}{dh}$ less negative than $-157N/km$. The gradient of $M$ is a useful indicator for the occurrence of ducting.

## 2.5 Forms of Atmospheric Refraction

(a) Negative Refraction $\frac{dN}{dh} > 0$ and $R$ is negative. The ray paths are curved upwards. The radio wave moves away from the earth's surface and the line of sight range and the range of propagation decreases accordingly.

(b) Zero refraction: $\frac{dN}{dh} = 0$ and $R$ is infinite. The ray is a straight line.

(c) Positive Refraction: $\frac{dN}{dh} < 0$ and $R$ is positive. The ray paths are curved towards the earth. Positive refraction can be subdivided into

(i) Standard: $\frac{dN}{dh} = -40N/km$, $k = 4/3$

(ii) Critical: $\frac{dN}{dh} = -157N/km$, $k = \infty$

(iii) Ducting: $\frac{dN}{dh} < -157N/km$, $k < 0$

The three broad classifications of atmospheric refraction are:

| Sub-refraction Region | Super refractive Region | Ducting Region |
|---|---|---|
| $\frac{dN}{dh} > -40$ | $-157 < \frac{dN}{dh} < -40$ | $\frac{dN}{dh} < -157$ |
| $\frac{4}{3} < k < 0$ | $0 < k < \frac{4}{3}$ | $k < 0$ |
| $\frac{dM}{dh} > 0$ | $\frac{dM}{dh} > 0$ | $\frac{dM}{dh} < 0$ |

**2.5.1 Super-refraction and ducting** Under the influence of synoptic processes such as subsidence, advection, or surface heating and radiative cooling, stratification can occur in the lower troposphere.

When $\frac{dN}{dh} < -157N/km$, we have ducting.

Ducting occurs for grazing angles of incidence, $\theta$ less than a critical angle $\theta_c$ (CCIR [7]).

$$\theta < \theta_c = \arcsin(\sqrt{2|\Delta M| \times 10^{-6}}) \tag{14}$$

where $\Delta M$ = change in $M$ across a ducting layer of thickness $\delta$.

For efficient duct propagation, $\lambda < \lambda_c$, where

$$\lambda_c = 1.9 \times 10^{-4} D^{1.8} \tag{15}$$

For an elevated duct, the duct thickness $D$ (metres) is given by (see Fig. 5)

$$D = \delta \left[ 1 + \left| \frac{dM}{dh} \right|_\delta \Big/ \left| \frac{dM}{dh} \right|_s \right] \tag{16}$$

where $|\frac{dM}{dh}|_\delta = \frac{\Delta M}{\delta}$ is the magnitude of the ducting gradient and $|\frac{dM}{dh}|_s$ = magnitude of the gradient in the underlying layer (if present). For a ground based duct with no underlying layer, $D = 2\delta$.

Tropospheric layers (e.g. near the surface) can



(i) introduce additional propagation paths, thus producing fading.

(ii) effectively isolate one communication terminal from the other e.g. as in Fig. 6 [11].

(iii) diffract the service propagation path, introducing losses.

(iv) cause interference to other distant services.

(v) result in leakage of secret communication.

**2.5.2 Surface and elevated ducts** The occurrence of initial gradient less than $-157$ $N$/km is used as a direct measure of the existence of ground based duct that is 100 m thick. The sea-surface ducts tend to be more prevalent and extensive than those overland. Fig. 7 shows the refractivity gradient contours for the trade wind inversion in May [10]. Fig. 8 shows the surface duct occurrence probability (%) in India for May and July at midnight [33]. The study of surface duct occurrence probability at six locations in West Africa carried out by Owolabi and Ajayi [27] showed that an average high surface ducting occurrence probability of 43% was found for three of the stations north of latitude 12°N compared with a corresponding probability of 8% for the three stations south of latitude 12°N. In general, Hautefeuille et al. [13] observed very deep fading of up to 50 dB on a 7 GHz radio link. Elevated ducts also occur in practice depending on the meteorological conditions.

## 2.6 Losses in Duct Propagation

The basic transmission loss is related to that of free space $L_{bf}$ by [6]

$$L_b = L_{bf} - 10 \log d' + A \tag{17}$$

where $d'$ = distance within the duct

$L_b$ = duct transmission loss

The factor $A$ accounts for other attenuation mechanisms such as leakage losses due to duct irregularities or losses due to ground reflection and etc. The free space path loss is given by

$$L_{bf} = 92.44 + 20 \log d + 20 \log f \tag{18}$$

with $d$ in km and $f$ in GHz.

## 2.7 Measurement of Radio Refractivity

(a) Direct method: The microwave refractomer is used. It is capable of measuring rapid fluctuations in $N$. The refractometer measures the change in the resonant frequency of a cylindrical cavity with ends open to the atmosphere and compares with the resonant frequency of a standard cavity sealed from the atmosphere. The refractometer is usually mounted on an aircraft for obtaining $N$–height profile, hence it is an expensive technique.

(b) Indirect method: $N$ can be computed from measured pressure, temperature and water vapour pressure.

(i) Tethered balloon system can be used for height profile in the first km of the troposphere. It has poor time resolution because each profile can take up to 1hr.

(ii) Meteorological sensors can be installed at intervals on a tower for measurement of the three parameters $p$, $T$ and $e$. It is only applicable to the lowest 200 m part of the atmosphere.

(iii) Upper air meteorological data measurements using radiosondes are carried out at some hundreds of stations all over the world, with launches at 0000 hrs GMT and 1200 hrs GMT. This system provides a large volume of data for statistical analysis, but the spatial and temporal resolutions of the data are poor for radio communication applications.

(c) Sodar: This is an acoustic sounding system, which is very useful for studying temperature inversions which cause radio ducts.

# 3. PRECIPITATION

The congestion in the low microwave frequency bands and the increasing need for high capacity communication channels have necessitated the use of frequencies above 10 GHz for both terrestrial and satellite communication systems. Hydrometers such as rain, hail, fog, ice, cloud and snow attenuate radio waves above 5 GHz and also cause other impairments to communication systems. The most important effects of hydrometeors on microwave propagation are [14]:

(a) attenuation caused by dissipation of radio wave energy as heat.



(b) scatter resulting in loss in the desired direction and consequently causing interference to other systems.

(c) depolarization due to the non–spherical nature of raindrops.

(d) rapid amplitude and phase scintillations caused by equivalent multipath propagation.

(e) antenna gain degradation due to phase dispersion of ray paths reaching the antenna.

(f) bandwidth coherence reduction especially in digital systems involving carriers spanning over large channel bandwidths.

## 3.1 Types of Rain

Stratiform rain – widespread regions with low rain rates and small embedded showers, with horizontal extent of hundreds of km and durations exceeding one hour. The rain vertical extent is up to the height of the bright band.

Convective Rain – localized regions of relatively intense rainfall characterized by strong up and down drafts extending deep into the troposphere. The horizontal scale is of several km and durations of tens of minutes.

Orographic – caused entirely or mostly by the forced uplift of moist air over high ground.

Monsoon Rain – a sequence of bands of intense convection followed by intervals of stratiform rain. The bands are typically 50km across, hundreds of km in length and produce heavy precipitation lasting for several hours.

Tropical Storms – Large regions of precipitation extending over hundreds of km. The storms are characterized by several spiral bands terminating in regions of intense precipitation surrounding the central region of the storm.

## 3.2 Drop Size Distribution

The three most commonly used distributions obtained mainly from temperate data are Laws and Parsons (L-P) [18], Marshall- Palmer (M-P) [20], Joss-Thunderstorm (J-T) and Drizzle (J-D)) [16].

The measurements of Laws and Parsons and Marshall and Palmer are fitted by a negative exponential of the form

$$N(D) = N_0 e^{-\Lambda D} \tag{19}$$

where

$$\Lambda = AR^{-0.21} \tag{20}$$

and $N(D)$ = number of drops per mm diameter interval per cubic metre, $N_0 = 8000 m^{-3} mm^{-1}$ and $A = 4.1$.

Joss et al. employed three classifications for rain events with different constants for the general exponential distribution given in Table 1.

The M-P distribution satisfies the rain rate equation making use of the fall velocity of the raindrops, but this is not true of the distributions of Joss et al. For example for $R$ of 100 mm/h used in the thunderstorm distribution, the true rain rate calculated from the volume of water falling is only 67 mm/h.

**3.2.1 Tropical raindrop size distribution** Making use of the raindrop size distribution measured in Nigeria, Ajayi and Olsen [2] proposed the following tropical model:

$$N(D) = \frac{N_T}{\sigma D\sqrt{2\pi}} \exp\left\{-\frac{1}{2}\left(\frac{\ell nD - \mu}{\sigma}\right)^2\right\} \tag{21}$$

where $\mu$ is the mean of $\ell nD$, $\sigma$ is the standard deviation, and $N_T$ is the total number of drops of all sizes.

$$N_T = 108 R^{0.363} \tag{22}$$

$$\mu = -0.195 + 0.199\ \ell nR \tag{23}$$

$$\sigma^2 = 0.137 - 0.013\ \ell nR \tag{24}$$

Fig. 9 shows the comparison between the M-P and the Ajayi-Olsen (A-O) distributions. The M-P overestimates both the small and the large diameter drop number for the tropical region.



**3.2.2 Shape of raindrops** For simplified calculations, spherical drops are assumed. However, falling drops assume a nearly spherical shape when subject only to the effects of gravity and the surface tension of water. The force of gravity provides the major orientation force for raindrops. The drops may vibrate and oscillate while falling, but the net shape is oblate spheroidal with the symmetry axis close to vertical. Pruppacher and Pitter [31] proposed a shape that is a function of drop size.

## 3.3 Rainfall Rate Distribution

A model for the rain rate distribution is given by [8]

$$P(R \geq r) = \frac{ae^{-ur}}{r^b} \qquad r \geq 2mm/h \tag{25}$$

where $a$ and $b$ are derived from the rain rate $R_{0.01}$ exceeded 0.01% of the time [21] and $u$ is the parameter depending on climate and geographical features.

$$a = 10^{-4} R_{0.01}^b \exp(uR_{0.01}) \tag{26}$$

$$b = 8.22 R_{0.01}^{-0.584} \tag{27}$$

and the values of $u$ given in Table 2 [22],[23] provide a good fit to the distributions observed at most locations. Fig. 10 shows CCIR rain climatic zones with values given in Table 3. Fig. 11 shows some cumulative rain rate distributions in tropical zone [23].

## 3.4 Rain Attenuation

Raindrops both absorb and scatter microwave energy. Both may contribute to the attenuation on a radio path, while scatter may also cause interference between radio paths. At wavelengths long compared with the drop size, attenuation due to absorption will be greater than that due to scatter, whilst at the shorter wavelenths, scatter will predominate. The Rayleigh scattering theory appears to apply only up to 3 GHz [15] while above 3 GHz, Mie scattering is the primary technique for rain attenuation calculations.

The specific attenuation $\gamma(dB/km)$ due to rain is given by

$$\gamma = 4.343 \int_0^\infty Q_t(D) \cdot N(D) dD \tag{28}$$

$Q(t)$ is the total extinction cross section.

$$Q_t(D) = Q_s(D) + Q_A(D) \tag{29}$$

where $Q_s$ and $Q_A$ are scattering and absorption cross sections respectively.

$Q_t(D)$ is a function of dropsize diameter, wavelength and complex refractive index $m$ of the water drops. $N(D)$ is the number of drops per unit volume per diameter interval.

The rain rate is related to the drop size distribution by

$$R = 6\pi \times 10^{-4} \int_0^\infty D^3 N(D) V(D) dD \tag{30}$$

where $V(D)$ = terminal velocity of drops in $ms^{-1}$ and $N(D)$ is in $mm^{-1}m^{-3}$.

The specific attenuation has been found to be related to rainfall rate $R$ as

$$\gamma = aR^b \tag{31}$$

where $a$ and $b$ are dependent on the frequency, polarization and the raindrop characteristics. The parameters $a$ and $b$ are available in form of Tables [7].

The analytical approximations for $a$ and $b$, adequate for system engineers are given by Olsen et al. [25].

$$\begin{aligned} a &= 4.21 \times 10^{-5}(f)^{2.42} \qquad 2.9 \le f \le 54GHz \\ &= 4.09 \times 10^{-2}(f)^{0.699} \qquad 54 \le f \le 180GHz \end{aligned} \tag{32}$$

and

$$\begin{aligned} b &= 1.41(f)^{-0.0779} \quad 8.5 \le f \le 25GHz \\ &= 2.63(f)^{-0.272} \qquad 25 \le f \le 164GHz \end{aligned} \tag{33}$$

where $f$ is in GHz.

Fig. 12 shows the comparison between the CCIR specific attenuation and those computed using Ajayi-Olsen tropical raindrop size distribution assuming spherical drops [1].

**3.4.1 Frequency scaling** When reliable long-term attenuation statistics are available at one frequency $f$, the attenuation of another frequency $f_2$ can be



estimated in the range 7 to $50GHz$, for the same hop length and in the same climatic region

$$\frac{A_1}{A_2} = \frac{g(f_1)}{g(f_2)} \tag{34}$$

where $A_1$ and $A_2$ are the values of attenuation in dB at frequencies $f_1$ and $f_2$ (in GHz) exceeded with equal probability. The function $g(f)$ is given by [8]

$$g(f) = \frac{f^{1.72}}{1 + 3 \times 10^{-7} f^{3.44}} \tag{35}$$

### 3.5 Rain Induced Depolarization

Terrestrial and earth-space microwave communication links could use two orthogonal polarizations at the same frequency to increase channel capacity and depolarization will limit the use of these two communication channels, as a result of the interferring crosstalk between the channels.

The cross polarization discriminations are given by

$$XPD_H = 20 \log |\Delta E_V / E_H| \tag{36}$$

$$XPD_V = 20 \log |\Delta E_H / E_V| \tag{37}$$

where $\Delta E_H$ = cross-polarized received field in the direction $E_H$ transferred from $E_V$, and $\Delta E_V$ is the cross-polarized received field in the direction $E_V$ transferred from $E_H$. $H$ and $V$ refer to horizontal and vertical polarizations respectively. The XPD is given by Oguchi [24] as

$$XPD_H = 20 \log \left| \frac{(1 - G) \tan\theta}{G + \tan^2\theta} \right| \tag{38}$$

$$XPD_V = 20 \log \left| \frac{(1 - G) \tan\theta}{1 + G \tan^2\theta} \right| \tag{39}$$

where $\theta$ = canting angle of raindrops and $G$ is given by

$$G = \exp[-(\Delta\alpha + j\Delta\phi)\ell] \tag{40}$$

where $\Delta\alpha$ = differential attenuation in nepers per unit length and $\Delta\phi$ is differential phase shift in degrees per unit length.

In terms of co-polarized path attenuation (CPA), we have [7]

$$XPD = U - V\log(CPA) \quad dB \tag{41}$$

where $U$ and $V$ depend primarily on $f(GHz)$, path elevation angle and polarization tilt angle (for linear polarization) relative to the horizontal. $U$ and $V$ also depend to some extent on drop size distribution, drop shape distribution and drop temperature. Fig. 13 shows the effect of raindrop shape on $XPD$ [4]. Spheroidal and Pruppacher and Pitter drop shapes were considered.

## 4. ATTENUATION BY ATMOSPHERIC GASES

Molecular absorption at centimetre and millimetre wavelengths is primarily due to atmospheric water vapour and oxygen. The oxygen molecule has a small magnetic moment and absorption is produced by magnetic interaction with the incident field. The interaction produces a series of very close lines between about 50 and 70 GHz and an isolated line at 119 GHz [9]. Oxygen does not change with latitude or season, but diurnal and seasonal variations of water vapour can be extremely large. The electric dipole associated with the water vapour molecule interacts with the electromagnetic radiation to produce rotation absorption lines at 22.2, 183.3 and 324 GHz. The thermal emission at frequencies near the peaks of the water vapour lines is also proportional to the number of water vapour molecules and may be used to sense the water vapour concentration when the temperature is known [34].

The total gaseous absorption in the atmosphere $A_a(dB)$ over a path length $r_0$ (km) is given by

$$A_a = \int_0^{r_0} \gamma_a(r)dr \tag{42}$$

where

$$\gamma_a(r) = \gamma_0(r) + \gamma_w(r) \tag{43}$$

$\gamma_a(r)$ is the specific attenuation $(dB/km)$ and $\gamma_0(r)$ and $\gamma_w(r)$ are the contributions by oxygen and water vapour respectively.

Fig. 14 [6] shows attenuation due to gaseous constitutents and precipitation for transmission through the atmosphere. Fig. 15 compares the CCIR and the values of specific attenuation computed for Nigeria [3].



### 4.1 Path attenuation

For terrestrial paths, the path attenuation is given by

$$A_a = \gamma_a r_0 = (\gamma_0 + \gamma_w)r_0 \tag{44}$$

where $r_0$ = path length.

For slant paths, the total attenuation is obtained by integrating equation (42) through the atmosphere.

For elevation angle $\theta$ greater than $10^0$

$$A_a = \frac{h_0\gamma_0 + h_w\gamma_w}{\sin\theta} \tag{45}$$

where $h_0$ and $h_w$ are oxygen and water vapour equivalent heights respectively.

The equivalent height concept is based on the assumption of an exponential atmosphere specified by a scale height to describe the decay in density with altitude. The equivalent heights for oxygen and water vapour may vary with latitude, season and/or climate.

An alternative approach based on surface meteorological parameters can be adopted. At the surface of the earth ($P = 1000mb$)

$$\gamma_a = a + b\rho - ct \tag{46}$$

where $\rho$ = surface water vapour concentration $g/m^3$

$t$ = surface temperature, $^0$C.

a,b,c are empirical coefficients derived by multiple regression analysis, which vary with operating frequency, $f$.

The total zenith attenuation $r_{90}$ based on the global data set is given by

$$r_{90} = \alpha + \beta\rho - \xi t \tag{47}$$

where $\rho$ = water vapour concentration at the surface $g/m^3$

$t$ = surface air temperature $^oC$.

$\alpha, \beta$ and $\xi$ are empirical coefficients from multiple regression, which are frequency dependent. The coefficients in equations are available in form of Tables [6].

For inclined paths the atmospheric attenuation may be assumed proportional to the effective distance through the attenuation medium as approximated by

$$r(\theta) = r_{90} \cdot \frac{r_a}{H_a} = \gamma_a r_a \tag{48}$$

where $r_a$ = effective slant path

$$r_a = \frac{2H_a}{\sqrt{\sin^2\theta + 2\frac{Ha}{n} + \sin\theta}} \qquad \theta \leq 10^0 \tag{49}$$

and

$$r_a = \frac{H_a}{\sin\theta} \qquad \theta > 10^0 \tag{50}$$

where $H_a$ = combined scale height of water vapour and oxygen.

$$H_a = r_{90}/\gamma_a \tag{51}$$

The attenuation on a slant path at an elevation angle $\theta$ from the surface to a height $h$ is given by

$$A_a = \gamma_a r_a |1 - \exp(-h/H_a)| \tag{52}$$

## 5. TERRESTRIAL LINE OF SIGHT

Some propagation problems to be taken into consideration are:

(i) diffraction fading due to obstruction of the path by terrain obstacles under adverse conditions of refractive index variation with height.

(ii) fading due to

(a) atmospheric multipath or defocussing associated with abnormal refractive layers.

(b) multipath from surface reflection

iii) attenuation due to

(a) rain and other hydrometeors

(b) atmospheric gases



iv) reduction in cross-polarization discrimination due to multipath and precipitation.

v) variation of the angle of arrival at the receiver terminal and angle-of-launch at the transmitter terminal due to refraction.

vi) signal distortion due to frequency selective fading and delay during multipath propagation.

### 5.1 Path Profile

An important factor when plotting a profile chart is the relative curvature of the earth and the microwave beam. This relative curvature can be shown graphically either as a curved earth with radius $ka$ and a straight line beam, or as a flat earth with a microwave beam having a curvature of $ka$. The latter method is preferred because of its flexibility.

Terrain has two effects on the propagation loss:

(i) Trees, buildings, hills or the earth can block a portion of the microwave beam to cause an obstruction loss.

This is a form of diffraction loss. The loss increases with decreasing path clearance from zero loss (i.e. free space conditions) to about 10 dB for zero clearance. The obstruction loss is zero for a path clearance of approximately $0.6F_1$, where $F_1$, the first Fresnel zone radius is given by

$$F_1 = 17.3\sqrt{\frac{d_1 d_2}{fd}} \tag{53}$$

where $f$ is frequency (GHz) and $d_1, d_2$ are distances from the link terminals in km, $d$ is the link length in km.

The $n^{th}$ Fresnel zone radius is given by

$$F_n = (n\lambda d_1 d_2/d)^{1/2} \tag{54}$$

Fig. 16 shows the CCIR recommendation for diffraction loss.

(ii) A very smooth section of terrain or water can reflect a second signal to the receiving antenna leading to loss and variation of received signal. Microwave paths with highly reflective terrain are undesirable and should be avoided when possible.

## 5.2 Planning Criteria for Path Clearance

The following procedure recommended by the CCIR can be adopted [8].

(i) Determine the antenna heights required for the appropriate median value of the point $k$- factor (in the absence of any data, use $k = 4/3$) and $1.0F_1$, clearance over the highest obstacle.

(ii) Obtain the value of $k_e(99.9\%)$ from Fig. 17 for the path considered.

(iii) Calculate the antenna heights required for the value of $k_e$ obtained from step (ii) and the following Fresnel zone clearance radii.

| *Temperature Climate* | *Tropical Climate* |
|---|---|
| $0.0F_1$(i.e. grazing) if there is a single isolated path obstruction<br>$0.3F_1$ if the path obstruction is extended along a portion of the path. | $0.6F_1$ for path lengths greater than about 30 km |

(iv) Use the larger of the antenna heights obtained by steps (i) and (iii).

## 5.3 Angles of Arrival

The variation of the angle of arrival in the vertical plane is appproximately proportional to the path length. The variations are caused by changes in the mean refractive index gradient. Deviations from the normal angle of arrival vary widely under multipath conditions and do not exhibit a strong dependence on path length.

## 5.4 Multipath Propagation

The presence of distinct propagation paths gives rise to variations in the received signal (amplitude and phase) in accordance with the mutual relationship between the amplitudes and phases of the separate signal contributions. The main effect is the generation of fades, which includes variations of the amplitude, the phase and the polarization of the received signal. Multipath fading (MPF) is a principal cause of outage in medium and high capacity microwave digital



radio systems. The diurnal and seasonal variations of multipath propagation are closely related to the occurrence of the meteorological conditions causing multipath propagation.

A general function for estimating the probability of fading is given by [35]

$$P(R \leq L) = K \cdot Q \cdot f^B \cdot d^C \cdot F_n^x \cdot L^2 \qquad (55)$$

where $P$ is the probability

$R$ and $L$ are amplitudes in linear measure.

$K$ is a factor for climatic conditions

$Q$ is a factor for terrain conditions

$f$ is the frequency (GHz)

$d$ is the path length in km

$F_n$ is a path clearance factor

$B, C$ and $x$ are constants.

In cases, where strong surface reflection has been prevented, the fading can be divided into 3 types:

(i) rapid scintillation – these are ususlly small amplitude fluctuations, which may not be significant and they are more noticeable at frequencies above 10 GHz.

(ii) slow non-selective fading due to single path propagation effects. It occurs during stratified atmospheric conditions and is less severe than multipath fading.

(iii) rapid frequency – selective fading due to multipath propagation. It is the most severe and governs the outage of analogue and digital radio links. Because the fading is frequency selective, the distortion induced at all amplitude levels in a wideband digital link can be a major source of outage. Multipath propagation reduces the cross-polarization isolation in a dual-polarized link.

Conditions for fade types (ii) and (iii) occur during the night and early morning hours of summer days in the temperate climates. In the tropics (especially at the costal locations), the fades have a higher incidence of occurrence.

**5.4.1 Diversity Improvement** Diversity system is used to reduce signal fading by selecting the highest level from two or more signal channels which carry the same information, but are taken from separate receivers, so long as the signals have a low cross-correlation. In frequency diversity, two different frequencies separated usually by less than 5% are used, whilst in space diversity two receiving channels are fed from two antennas spaced a distance apart. Vertical spacing of about $150\lambda$ is desirable for space diversity to be effective. In quadruple channel diversity the combination of frequency and space diversities is utilized. In angle diversity use is made of two or more antenna beams separated by small angles in the vertical plane. In areas where ducting is prevalent e.g. in Senegal and parts of West Africa [13] measurements indicate that diversity using parallel radio paths properly spaced above the ground could lead to significant improvement in reception.

## 5.5 Path Attenuation due to Precipitation

The effective path length technique is one of the methods used to account for the spatial inhomogeneity of precipitation along a microwave link in the calculation of the total path attenuation due to precipitation, using the point surface rain rate. The path attenuation $A_{0.01}$ exceeded for 0.01% of the time is given by

$$A_{0.01} = \gamma \cdot \ell_{eff} = \gamma \cdot r \cdot L \tag{56}$$

where $\gamma$ is the specific attenuation at the frequency, polarization and surface rain rate, $L$ is the physical length of the path and $r$ is the reduction factor, given by [8]

$$r = \frac{1}{1 + 0.045L} \tag{57}$$

For percentages of time, $p$ between 0.001 and 1.0, the path attenuation $A_p$ is given by [8]

$$\frac{A_p}{A_{0.01}} = 0.12p^{-(0.546+0.043 \log P)} \tag{58}$$

These CCIR recommendations are based on results obtained in Europe, Japan and USA. For simultaneous rain rate and attenuation measurements, mean error is about $-5\%$ and standard deviation between 10 and 15% as a function of percentage of time.



# 6. EARTH-SATELLITE PATH

## 6.1 Vertical Structure of Precipitation

A vertically homogeneous and cylindrical model of a raincell extending from the earth's surface to the $0°C$ isotherm height has been assumed in prediction models for attenuation. Although the simple raincell model has given good results for the temperate latitudes, it overestimates the attenuation in the tropical regions because of the heavy rainfall, different character of tropical rain with different horizontal and vertical structure and/or different drop size distributions.

Below the 0°C isotherm liquid particles exist, that attenuate the signals and above the $0°C$ isotherm, there are only freezing particles with negligible attenuation on the radio waves.

The average height of the 0°C isotherm, $h_{FR}$ during rainy conditions is given by [8]

$$h_{FR} = \begin{cases} 4.0 & \text{for } 0 < \phi < 36° \\ 4.0 - 0.075(\phi - 36) & \text{for } \phi \geq 36° \end{cases} \tag{59}$$

where $\phi$ is the latitude (degrees).

Ajayi and Odunewu [5] have shown that $h_{FR}$ obtained in Nigeria is generally higher than the CCIR values. The effective rain height, $h_R$ for prediction of attenuation is in general different from the 0°C isotherm height. For Europe, $h_R \approx h_{FR}$.

## 6.2 Average Year Path Attenuation due to Precipitation

With reference to Fig. 18, the slant path, $L_s$ below the rain height is given by

$$L_s = \frac{h_R - h_S}{\sin\theta} \quad km \qquad \theta \geq 5° \tag{60}$$

$$L_s = \frac{2(h_R - h_S)}{(\sin^2\theta + 2\frac{h_R - h_S}{Re})^{1/2} + \sin\theta} \quad km \qquad \theta < 5° \tag{61}$$

where $h_S$ is the height above mean sea level of the earth station and $Re$ is the effective radius of the earth (8500 km).

The horizontal projection, $L_G$ of the slant path is given by

$$L_G = L_s \cos\theta \tag{62}$$

where $\theta$ is angle of elevation.

For a rain rate, $R_{0.01}$ exceeded for 0.01% of time the specific attenuation is given by

$$\gamma_R = a(R_{0.01})^b \tag{63}$$

The slant path attenuation exceeded for 0.01% of an average year is given by [7]

$$A_{0.01} = \gamma_R \cdot L_e \cdot r_{0.01} \tag{64}$$

where $r_{0.01}$, the reduction factor for 0.01% of time is given by

$$r_{0.01} = \frac{1}{1 + 0.045 L_G} \tag{65}$$

For other percentages of an average year, the attenuation $A_p$ exceeded is given by

$$\frac{A_p}{A_{0.01}} = 0.12 P^{-(0.546 + 0.043 \log P)} \tag{66}$$

For latitudes, $\phi > 30°$, the prediction is in agreement within 10% of measurements at 0.01% level. However for low latitudes the prediction overestimates and the predicted value is to be divided by 3 in order to obtain values comparable with available measurement data. The available attenuation data for low latitudes are few, hence it is difficult to ascertain what percentage of the overestimation is due to the prediction technique and that due to attenuation measurement error.

Intense raincells responsible for large attenuation usually have horizontal dimensions of a few km, hence site diversity is employed to improve system reliability. Orbital diversity is also being investigated as a possible method of improving system reliability.

## 7. TRANSHORIZON PROPAGATION

This can be broadly divided into two parts:

(i) Provision of radio relay systems

(ii) Intersystem Interference



### 7.1 Radio Relay Systems

For frequencies greater than 30MHz, beyond the horizon propagation which occur permanently are due to

(a) diffraction – attenuation increases rapidly with distance, hence not suitable

(b) scatter from atmospheric irregularities – used to establish transhorizon radio communication.

Such systems require high power transmitters, high gain antennas, sensitive receivers and usually some diversity system to overcome signal fading. The practical frequency range is about 200 MHz to 5GHz and up to distances of about 1000 km.

**7.1.1 Long term median transmission loss** The long term median transmission loss, $L(50)$ due to tropospheric scatter has the form [6]

$$L(50) = 30 \log f - 20 \log d + F(\theta d) - G_t - G_r + L_c - V(d_e) \text{ in } dB \tag{67}$$

where $f$ is frequency (MHz), $G_t$, $G_r$ are antenna gains, $L_c$ is the aperture to medium coupling loss (or gain degradation) of the two antennas, $\theta$ (radians) is the angle between the radio horizon in the great circle plane containing the path terminals for median atmospheric conditions, $F(\theta d)$ is a function of the angle $\theta$(radians) and the distance $d(km)$, shown in Fig. 19 as a function of the surface refractivity $N_s \cdot V(d_e)$ is a correction for various types of climates [6]. A semi-empirical estimate of $L_c$ is given by

$$L_c = 0.07 \exp[0.055(G_t + G_r)] \quad dB$$

$$G_t < 50dB, \; G_r < 50dB \tag{68}$$

In terms of the radiometeorological parameters, the basic transmission loss $L_b(P)$ for the time percentage $P$, in $dB$ can be obtained from the semi-empirical formula [6]

$$L_b(P) = 102 + 30 \log d + 30 \log f + 1.5 G_c \tag{69}$$

where $d$ is distance (km), $f$ is frequency $(MHz)$ and $G_c$ is the gradient near the base of the common volume, which can often be replaced by the difference between the value of $N$ at 1 km above and at the base of the common volume.

**7.1.2 Signal Variations** Slow variations are due to major changes in refractive index and are weather dependent. They are not strongly dependent on frequency. Rapid fading is a result of the vector addition of many incoherent contributions (i.e. with different amplitude and phase) from a large number of scattering elements within the common volume of the two antennas of the radio link. The rapidly varying fading pattern determine the transmissible bandwidth, the associated limitations to rate of transfer of digital data and the gain degradation of the antennas that may be expected.

Quadruple diversity is widely used to overcome rapid fading effects in order to achieve operational reliability of about 99.9%. Frequency/angle diversity can be employed, in which only one antenna is used at each end of the link, but two vertically spaced feeds to the receiver antenna so as to give offset beams. Such a technique is useful where large antennas and high land costs are involved or on offshore oil rig platform.

### 7.2 Intersystem Interference

Fig. 20 shows [9] the propagation phenomena producing interference. The high level fields produced by ducting and rain scatter cause intersystem interference. Rain scatter on a space-Earth path can cause interference to a terrestrial system. Scatter from a terrestrial link to a space station is also possible. The scattering can be considered to be approximately isotropic and maximum coupling will occur when the main lobes (of the space station and terrestrial station) intersect in rain.



## REFERENCES


1) Ajayi G.O., "*Characteristics of rain induced attenuation and phase shift at cm and mm waves using a tropical raindrop size distribution model*", Int.J. Infrared and mm waves **6**, 771-806 (1985).

2) Ajayi G.O. and Olsen R.L., "*Modelling of a tropical raindrop size distribution for microwave and millimetre wave applications*", Radio Science **20**, 193-202 (1985).

3) Ajayi G.O. and Kolawole L.B., "*Centimeter and millimeter wave attenuation by atmospheric gases and rainfall at a tropical station*", Int. J. of Infrared and mm. waves, **5**, 919-935 (1984).

4) Ajayi G.O., Owolabi I.E. and Adimula I.A., "*Rain induced depolarization from 1GHz to 300 GHz in a tropical environment*", Int.J. Infrared and mm waves **8**, 177-197 (1987).

5) Ajayi G.O. and Odunewu P.A., "*Some characteristics of the rain height in a tropical environment*", IEE Int. Conf. Antennas and Propag. (Warwick, UK, April 1989).

6) CCIR, Recommendations and Reports of the International Radio Consultative Committee, XVth Plenary Assembly - Propagation in non-ionized media, Vol. V (1982).

7) CCIR, Recommendations and Reports of the International Radio Consultative Committee, XVIth Plenary Assembly - Propagation in non-ionized media, Vol. V (1986).

8) CCIR, Conclusions of the Interim Meeting of Study Group 5 - Propagation in non-ionized media, DOC 5/204-E (July, 1988).

9) Crane R.K., A review of transhorizon propagation phenomena URSI Comm. F. Open Symp. (Lennoxville, Quebec, Canada, 1980).

10) Dougherty H.T., Riggs L.P. and Sweezy W.B., "*Characteristics of the Atlantic trade wind system significant for radio propagation*", Technical Report 29, US Dept. of Commerce, (Institute of Telecommunications Sciences, 1967).

11) Dougherty H.T. and Dutton E.J., "*The role of elevated ducting for radio service and interference fields*", US Dept. of Commerce, NTIA Report -81-69 (1981).

12) Hall M.P.M., "*Effects of the troposphere on radio communication, Institution of Electrical Engineers*" (London, 1979).

13) Hautefeuille M., Boyle A.W. Timmers A.W. and Shannon J.D., "*Ducting fading - is Senegal an isolated case?*" Telecommunication Journal **47**, 517-525 (1980).

14) Ippolito L.J., Radio propagation for space communication systems, Proc. IEEE 69 (1981).

15) Ippolito L.J., Kaul R.D. and Wallace R.G., *Propagation Effects Handbook for Satellite Systems Design, A Summary of Propagation Impairments on 10 to 100 GHz satellite links with techniques for system design.* NASA, USA Reference Publication **1082** (03) (1983).

16) Joss J., Thams J.C. and Waldvogel A., "*The variation of raindrop size distributions at Locarno*", Proc. Int. Conf. Cloud Phys., Toronto, Canada 369-373 (1968).

17) Kolawole L.B. and Owonubi J.J. "*The surface radio refractibvity over Africa*", Nigerian Journal of Science **16**, 441-454 (1982).

18) Laws J.O. and Parson D.A., "*The relation of raindrop size to intensity*", Trans. Amer. Geophys. Union **24**, 452-460 (1943)

19) Lenkurt, Microwave Path Engineering Considerations 6000 - 8000 MC USA (1960).

20) Marshall J.S. and Palmer W.M., "*The distribution of raindrops with size*", J. of Meteoroloy USA **5**, 165–166 (1948).

21) Moupfouma F., "*Model of rainfall rate distribution for radio system design*", IEE Proc. 132 Pt. H 39–43 (1985).

22) Moupfouma F. Atlas mondial des intensities de pluie en 1 minute, note Tech. CNET (MER/RPE), France (1985).

23) Moupfouma F., "*More about rainfall rates and their prediction for radio systems enineering*" Proc. IEE Part H 134, 527–537 (1987).



24) Oguchi T., "*Electromagnetic wave propagation and scattering in rain and other hydrometeors*", Proc. IEEE 71, 1029-1078 (1983).

25) Olsen R.L., Rogers D.V. and Hodge D.B., "*The $aR^b$ relation in the calcultion of rain attenuation*", IEEE Trans. Ant. and Propagation AP-26 318-329 (1978).

26) Owolabi I.E. and Williams V.A., "*Surface radio refractivity patterns in Nigeria and the Southern Cameroons*", J. West African Science Association **15**, 3–17 (1970)

27) Owolabi I.E. and Ajayi G.O., "*Superrefractive conditions and their implication for tropospheric rdio-wave propagation in West Africa*", Nigerian Journal of Science **10**, 291-313 (1976).

28) Oyinloye J.O., "*The troposphere in tropical and subtropical latitudes*" in *Handbook on Radiopropagation for tropical and subtropical countries*, 79–99 (1987).

29) Oyinloye J.O., "*Characteristics of non-ionized media and radiowave propagation in equatorial areas*", A review, Telecomm. Journal **55**, 115-129 (1988).

30) Pontes M.S. and Assis M.S., "*Propagation conditions in South and Central America*", Paper presented to the preparatory Seminar for 1983 WARC 1981.

31) Pruppacher H.R. and Pitter R.L., "*A semiempirical determination of the shape of cloud and raindrops*", J. Atmos. Sci. **28**, 86–94 (1971).

32) Radicella S.M., "*Tropospheric radio propagation, Autumn Course on geomagnetism, the ionosphere and magnetosphere*", SMR/98 –48, ICTP, Trieste, Italy 1982.

33) Reddy B.M., "*Characterization of tropospheric environment, Autumn Course on geomagnetism, the ionosphere and magnetosphere*", SMR/98-44, ICTP, Trieste, Italy (1982).

34) Reddy B.M., "*The Physics of the Troposphere*" in *Handbook on Radiopropaation for tropical and sub-tropical countries* (1987).

35) Stephensen E.T., "*Review of Clear-air propagation on line-of-sight radio paths*" URSI Comm. F. Open Symp. Lennoxville, Canada, 1980.

Table 1
Joss et al. classification of rainfall

| Type of rain | $N_0$ | A |
|---|---|---|
| Drizzle | 30,000 | 5.7 |
| Widespread rain | 8,000 | 4.1 |
| Thunderstorm rain | 1,400 | 3.0 |



Table 2
Classification of parameter u values [23]

| Localities | Temperate zones | | | | | Tropical zone |
|---|---|---|---|---|---|---|
| | EUROPE | | AMERICA | | JAPAN | |
| | Central Southern | Northern | Canada | USA | | |
| – Coastal or nearby water masses and mountainous regions | 0.030 | 0.045 | 0.032 | 0.032 | 0.045 | 0.042 |
| – Average rolling terrain | 0.025 | 0.025 | 0.025 | 0.025 | 0.045 | 0.025 |
| – Arid regions | | | 0.015 | 0.015 | | |

Table 3

CCIR Rain climatic zones [7)]

Rainfall intensity exceeded (mm/h) Reference to Fig. 10.

| Percentage of time (%) | A | B | C | D | E | F | G | H | J | K | L | M | N | P |
|---|---|---|---|---|---|---|---|---|---|---|---|---|---|---|
| 1.0 | - | 1 | - | 3 | 1 | 2 | - | - | - | 2 | - | 4 | 5 | 12 |
| 0.3 | 1 | 2 | 3 | 5 | 3 | 4 | 7 | 4 | 13 | 6 | 7 | 11 | 15 | 34 |
| 0.1 | 2 | 3 | 5 | 8 | 6 | 8 | 12 | 10 | 20 | 12 | 15 | 22 | 35 | 65 |
| 0.03 | 5 | 6 | 9 | 13 | 12 | 15 | 20 | 18 | 28 | 23 | 33 | 40 | 65 | 105 |
| 0.01 | 8 | 12 | 15 | 19 | 22 | 28 | 30 | 32 | 35 | 42 | 60 | 63 | 95 | 145 |
| 0.003 | 14 | 21 | 26 | 29 | 41 | 54 | 45 | 55 | 45 | 70 | 105 | 95 | 140 | 200 |
| 0.001 | 22 | 32 | 42 | 42 | 70 | 78 | 65 | 83 | 55 | 100 | 150 | 120 | 180 | 250 |



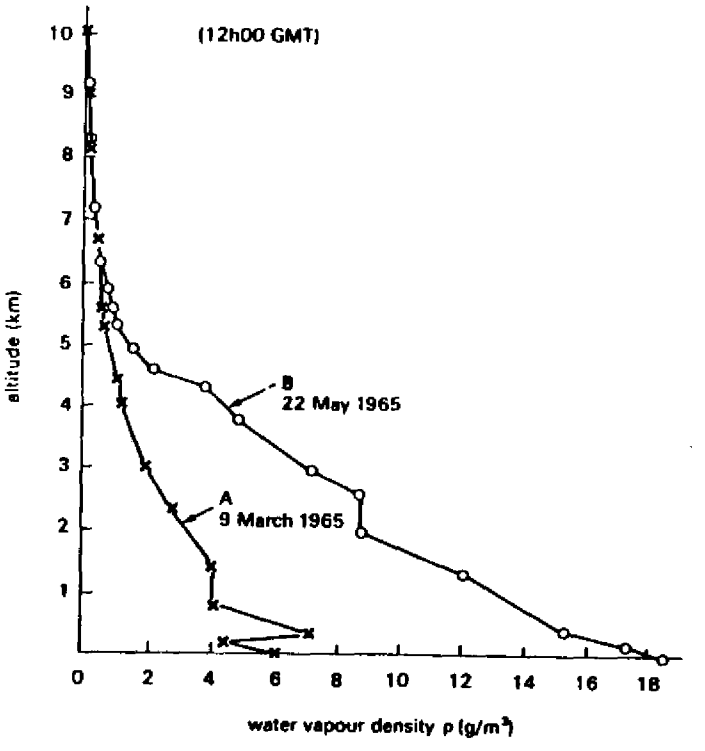


Fig.1

Variation of water vapour concentration with altitude at Niamey in Niger (from Ref. 28).

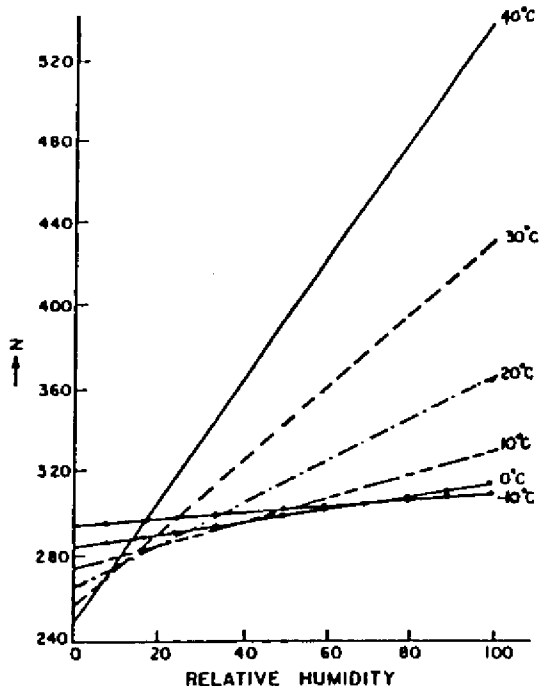


Fig.2

Calculated values of radio refractivity plotted against relative humidity at different temperatures (after Ref. 34).



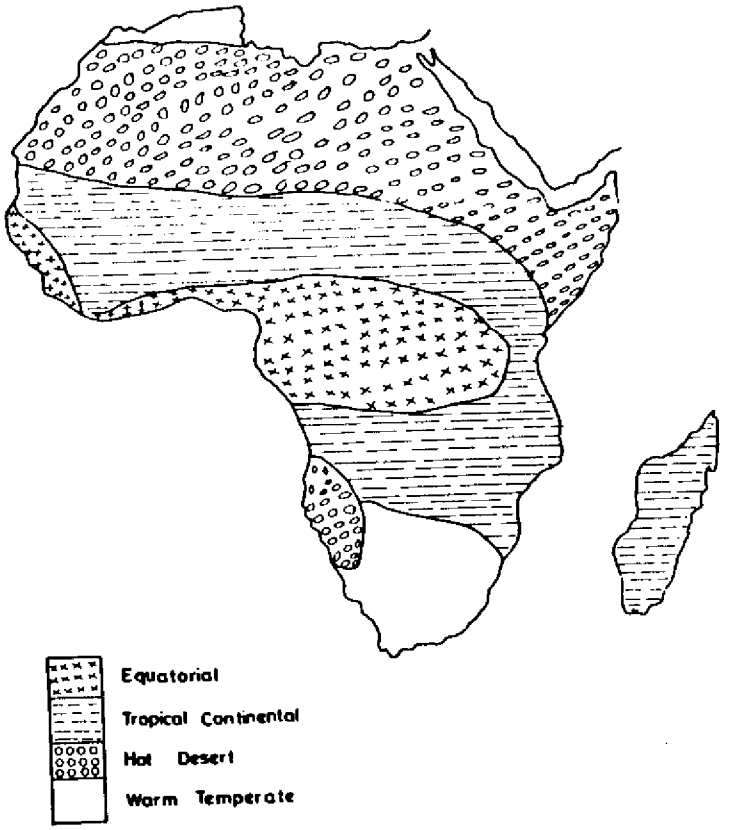


Fig.3(a)

Main climatic regions of Africa (after Ref.17).

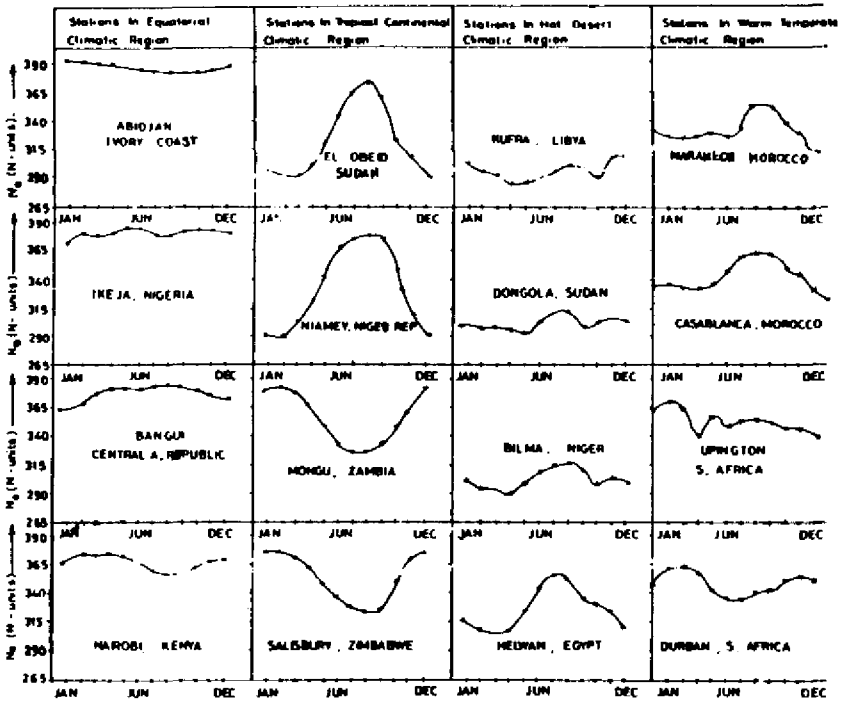


Fig.3(b)

**No patterns in the different climatic regions of Africa (after Ref. 17).**



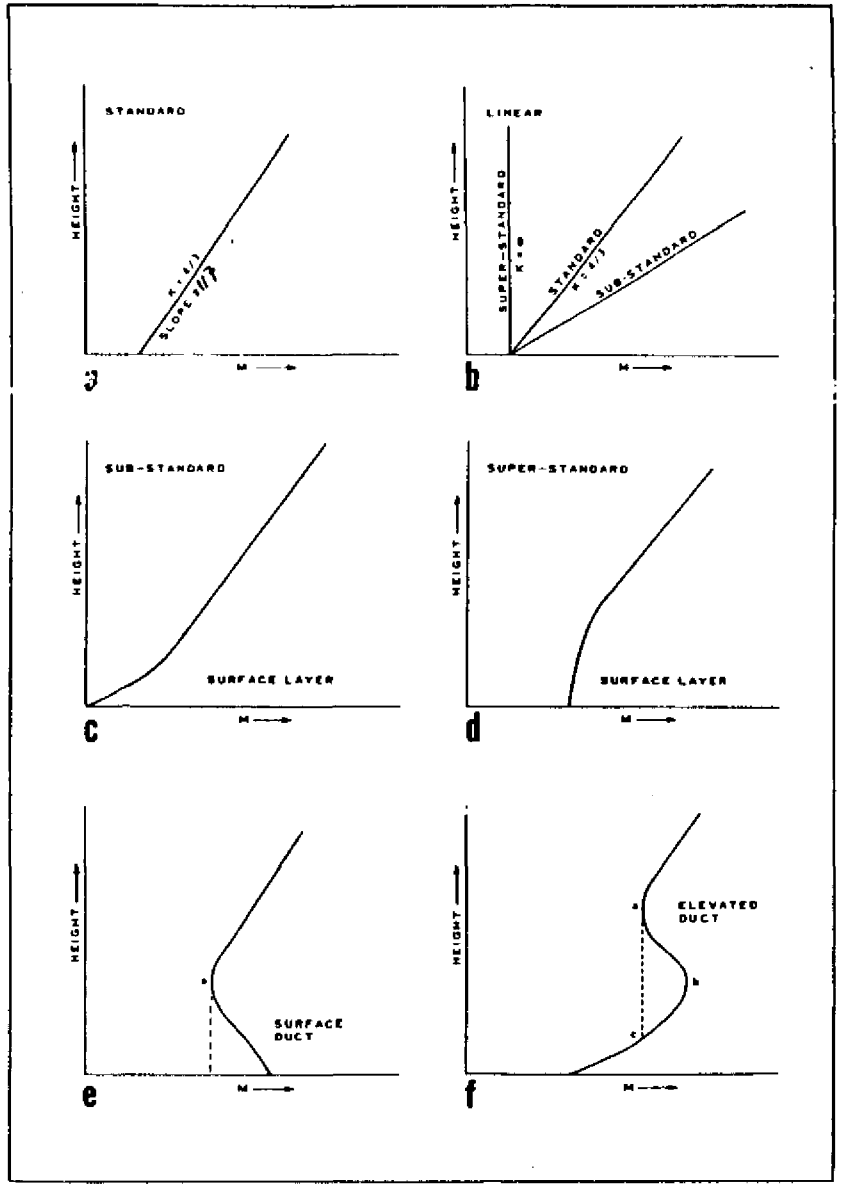


Fig.4

**Typical $M$ profiles (after Ref. 19).**

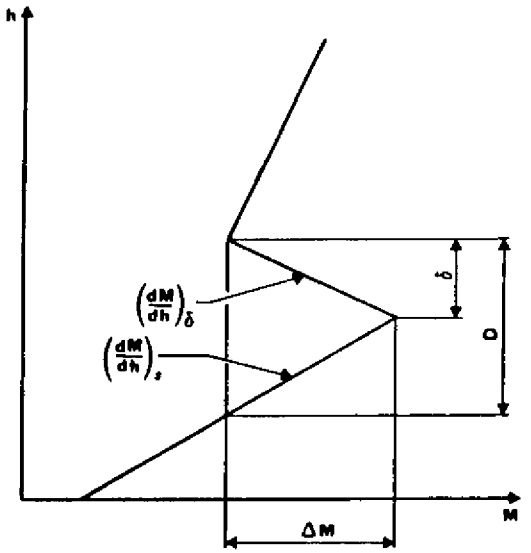


Fig.5

Radiometric characteristics of a ducting layer [6]
$\delta$: ducting layer thickness
D: tropospheric radio duct thickness.



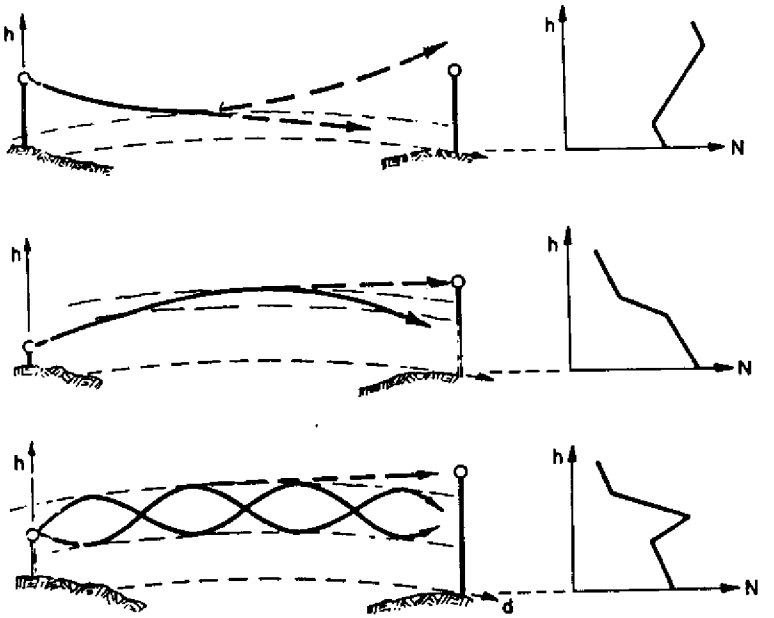


Fig.6

An atmospheric fading mechanism, isolation. Isolation of terminals, one from another may be caused by atmospheric layers and ducts (after Ref. 11).

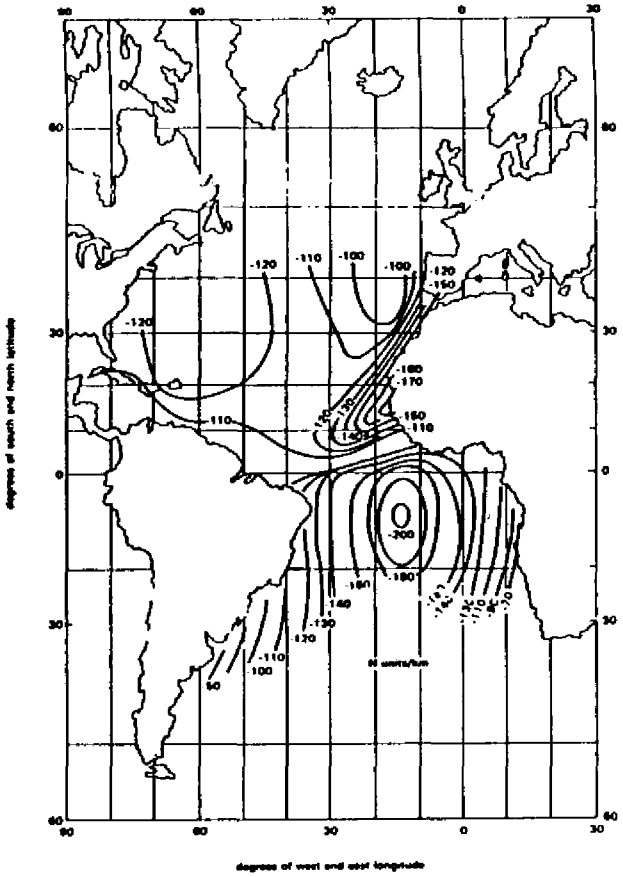

Fig.7

Refractivity gradient contours for the trade wind inversion in May (after Ref. 10).



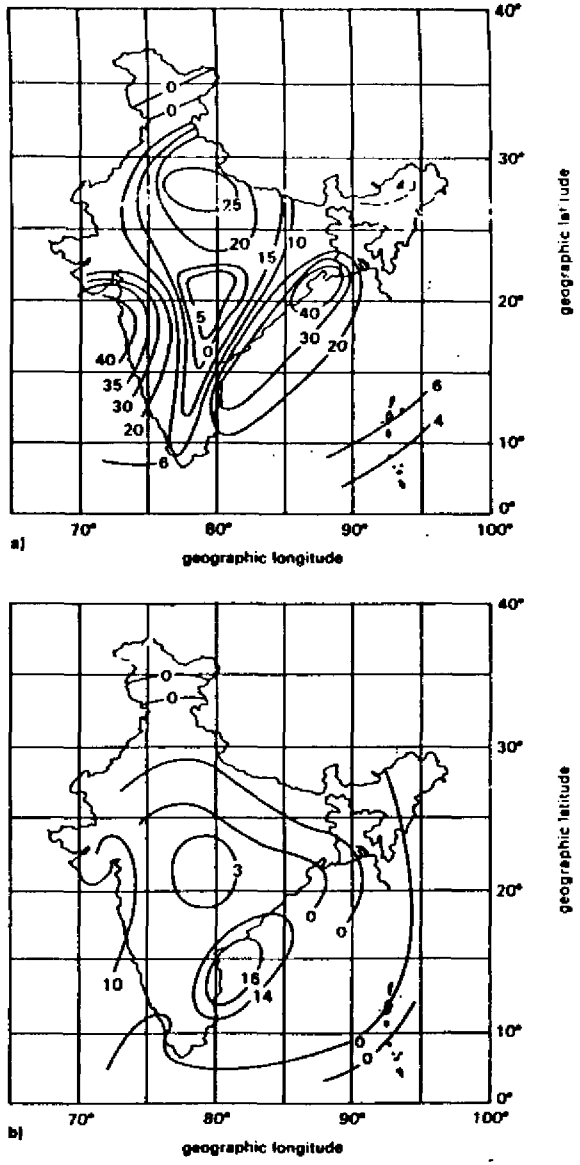


Fig.8

Surface duct occurrence probability (%) in India for a) May and b) July at 00h00 GMT (after Ref.33).

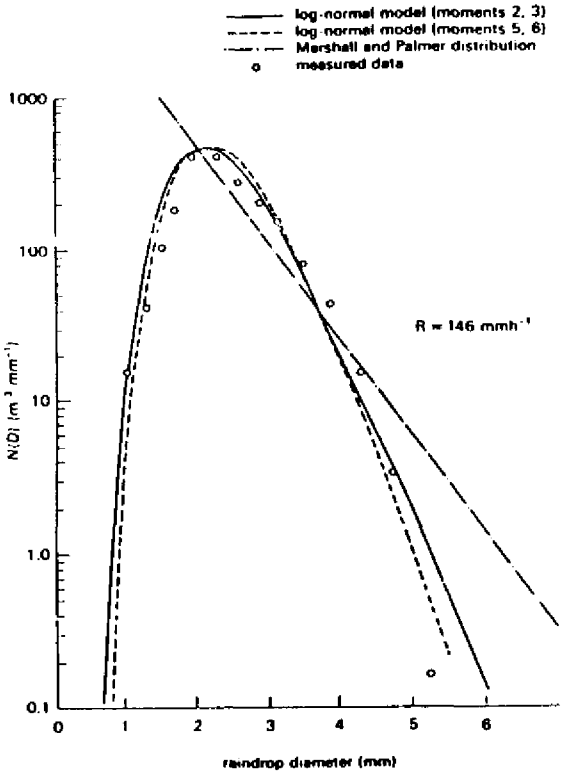


Fig.9

Comparison of Ajayi-Olsen raindrop size lognormal model with the Marshall and Palmer distribution (after Ref. 2).



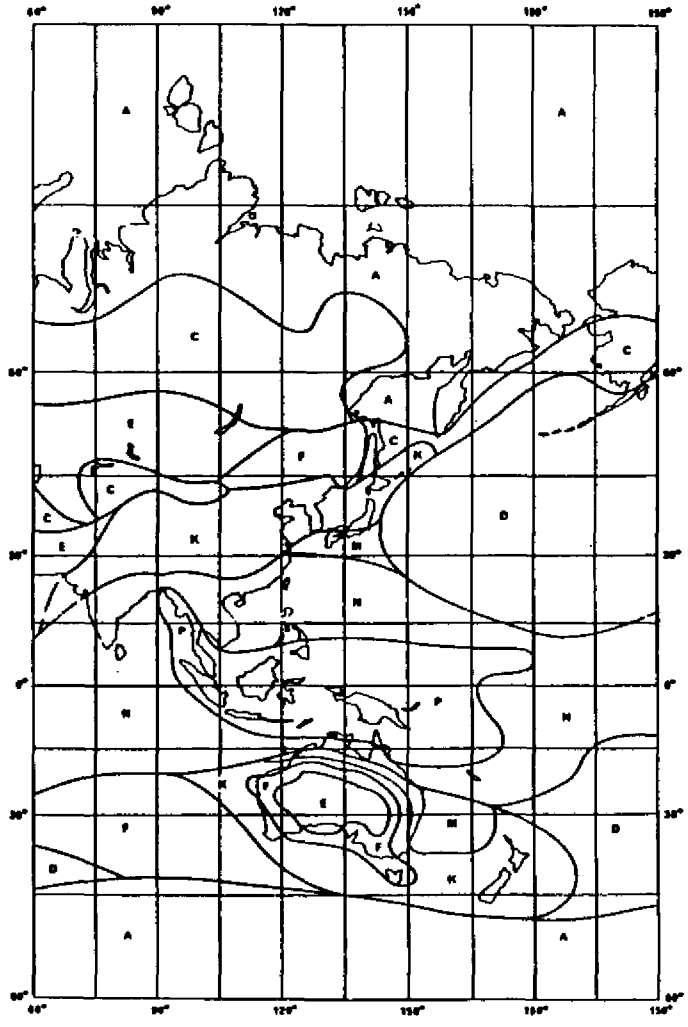

Fig.10

Rain climatic zones (refer to Table 3) [7].

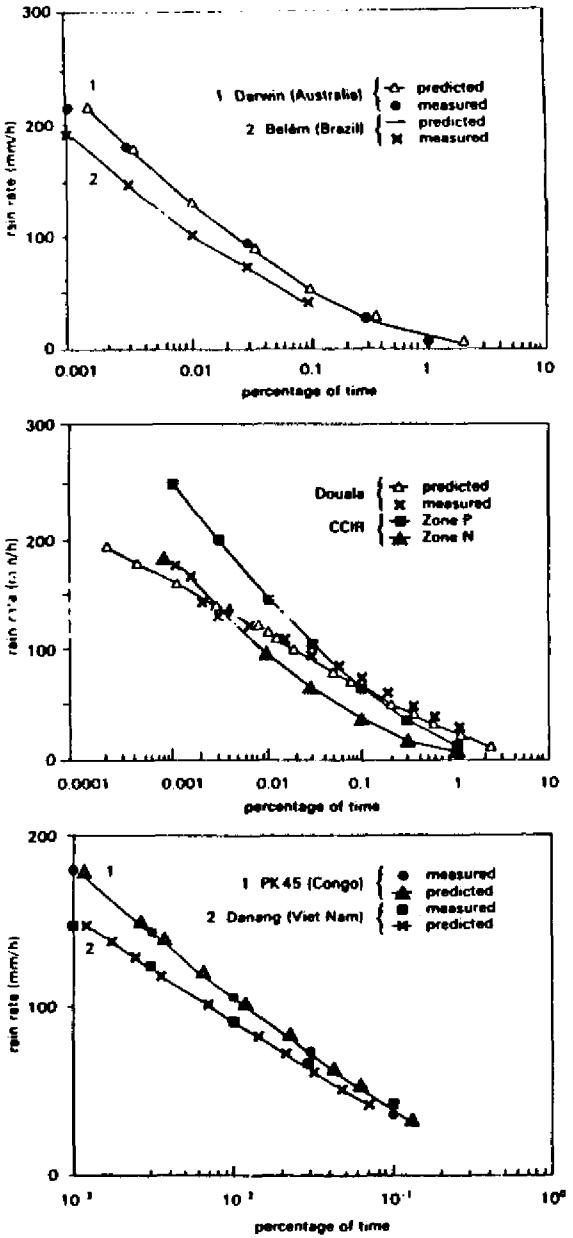


Fig.11

Cumulative rain rate distribution in tropical zones (after Ref. 21).



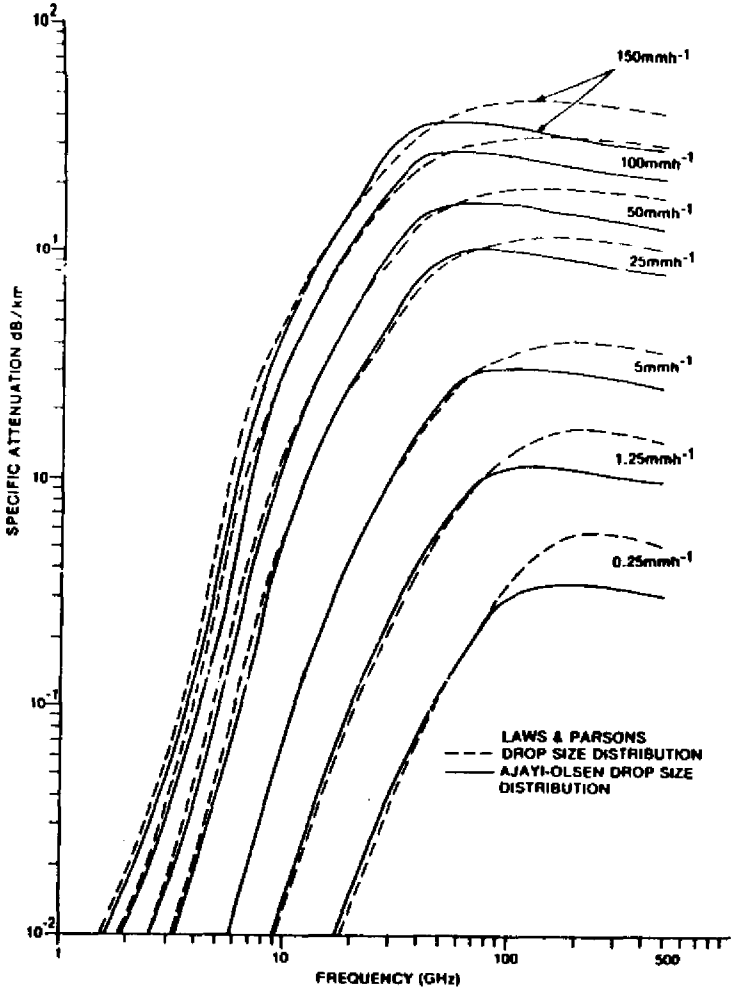


Fig.12

Specific attenuation assuming spherical raindrops at 20°C (after Ref. 1).

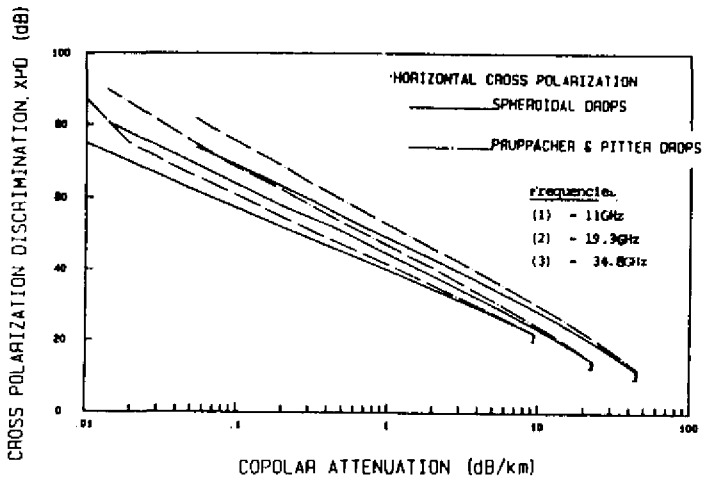


Fig.13

Variation of cross polarization discrimination, XPD with copolar attenuation CPA at three frequencies showing the effect of raindrop shape (after Ref. 1).



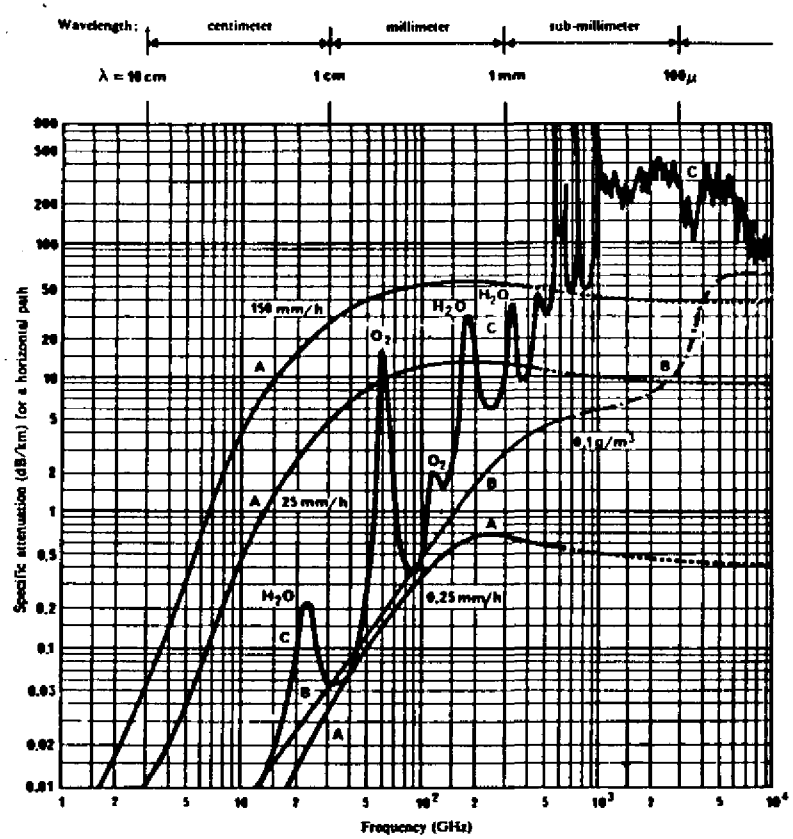


Fig.14

Attenuation due to gaseous constituents and precipitation for transmissions through the atmosphere [6].

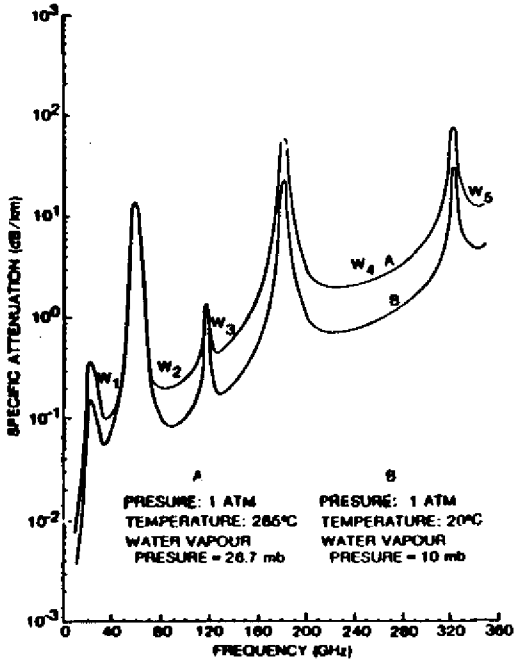


Fig.15

Specific attenuation due to oxygen and water vapour (after Ref. 3).



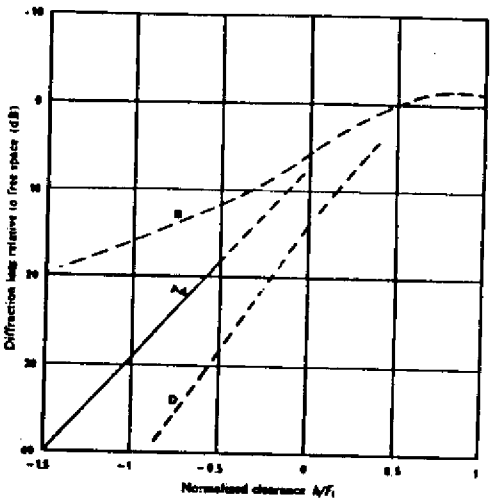


Fig.16

Diffraction loss for obstructed line-of-sight microwave radio paths [6].

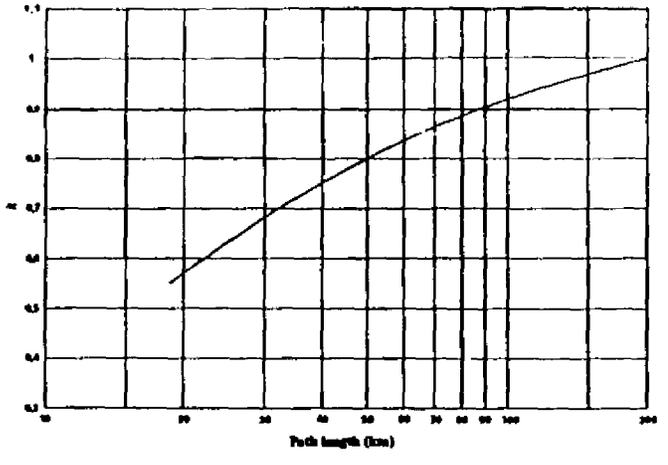

Fig.17

Minimum effective value of $k$ exceeded for approximately 99.9% of the time (Continental temperate climate) [6)]



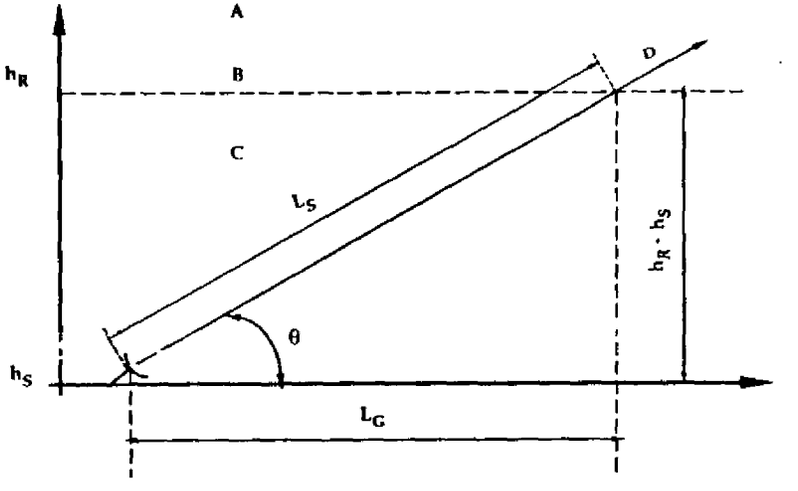


Fig.18

Schematic representation of an Earth-space path

A. Frozen precipitation

B.Rain height

C.Liquid precipitation

D.Earth-space path

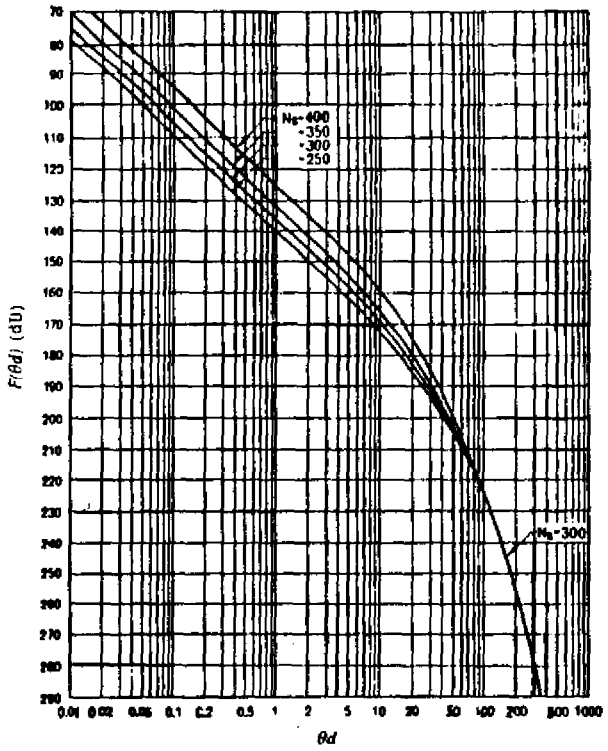


Fig.19

The attenuation function $F(\theta d)$, where $d$ is in km and $\theta$ in radians [6].



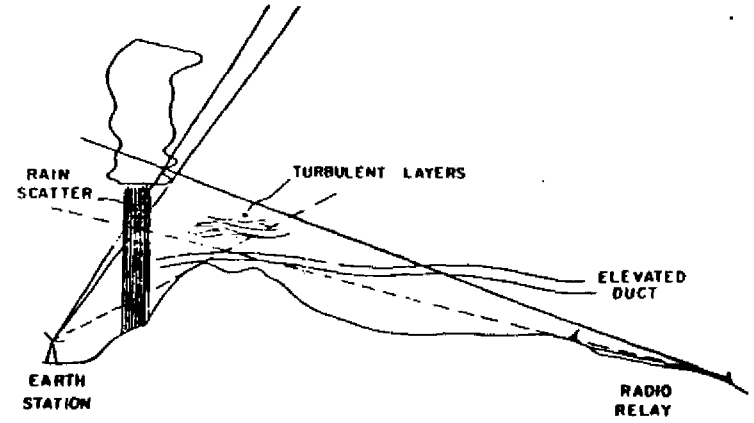


Fig.20

Propagation phenomena producing interference [9].